

Atomic Resolution in Lensless Low-Energy Electron Holography

Hans-Werner Fink and Heinz Schmid

IBM Research Division, Zurich Research Laboratory, 8803 Rüschlikon, Switzerland

Hans Jürgen Kreuzer and Andrzej Wierzbicki

Department of Physics, Dalhousie University, Halifax, Nova Scotia, Canada B3H 3J5

(Received 21 June 1991)

With the low-energy-electron projection microscope it has been possible to image the lattice of thin gold films with atomic resolution. A theory modeling the coherent point source as the origin of a spherical wave is capable of describing both the Gabor-type holograms as well as the atomically resolved lattice images of the gold films.

PACS numbers: 61.16.Di, 07.80.+x

More than 40 years ago, Gabor [1] proposed a new principle for electron microscopy. His vision was to circumvent the limitations of electron lenses by recording both the amplitude and phase information of the scattered wave from an object. This record, an interference pattern, has been named "hologram" since it contains the entire information of the scattered wave front at the object. Necessary for such a microscopy scheme are a coherent ensemble of particles with wave nature that provides a coherent background at some two-dimensional detector, an object that scatters the wave elastically to preserve the coherence with the reference wave, and finally a way to magnify the hologram, which is created by the interference of the reference and the object wave.

The invention of the laser made holography an established technique in light optics. For electrons, with about 4 orders of magnitude smaller wavelengths, the development of holography was slow due to both the lack of coherent sources and the aberrations of the lens system necessary to magnify the hologram. Only recently and with significant technical effort has electron holography become a vital tool in electron microscopy as demonstrated by the work of the Tübingen and Hitachi groups [2].

We have devised a scheme for electron holography that employs a coherent divergent electron beam directly without the need for a lens system. The key to this scheme is an ultrasharp tip that can ultimately be shaped into a single-atom tip by field-ion microscopy techniques [3] and that acts as a coherent point source for electrons. With this it has been possible to image the lattice of thin gold films with atomic resolution. A straightforward theory has been developed that allows us to predict the essential features of the holograms by including the proper experimental geometry and the nature of the scattering potential for carbon fibers and thin gold films.

Two kinds of experiments and the corresponding model calculations will be presented; they are schematically illustrated in Fig. 1.

(a) Gabor-type holography, in which the object, placed in the divergent electron beam, covers only a small part of the beam. This situation is illustrated in Fig. 1(a).

Experimentally this is realized by placing the ultrasharp tip at a submicron distance from a perforated carbon film containing small fibers crossing the holes. The hologram of the fibers is observed at a two-dimensional electron detector 10 cm away. Owing to the close proximity between tip and sample, electron energies between 20 and 80 eV can be achieved.

(b) In transmission holography, the divergent beam "illuminates" a thin gold film and the transmission image is observed at the distant detector. Here the object covers most of the primary wave as indicated in Fig. 1(b). Imaging is done only with the elastic transmitted electrons, which implies a need for a higher primary current. The electron energies in transmission microscopy are between 150 and 300 eV.

In the experiments the tip is brought into close proximity of the sample by orthogonal "inch worms" that allow

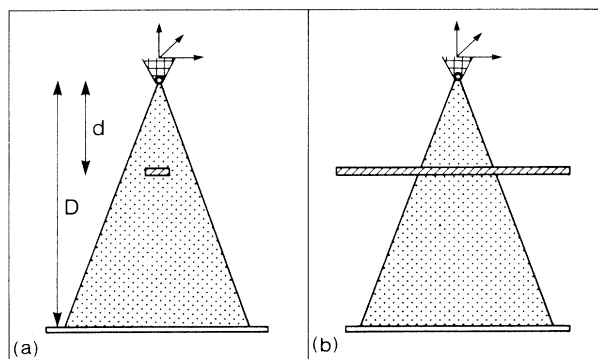


FIG. 1. With the low-energy-electron projection microscope two closely related types of experiments have been performed: (a) Gabor-type holography, where the sample covers only part of the divergent electron beam, while most of the reference wave misses the sample. (b) Transmission microscopy, where a thin film interacts with all of the electrons emitted from the point source. To achieve a high magnification, the sample is placed at a microscopic distance d from the source and the image is observed at a detector placed a macroscopic distance D away from the source.

motion over several millimeters. For the fine approach piezo scanners are used. Images are taken at a TV rate. A more detailed description of the technique is given in Ref. [4].

In the model for low-energy-electron projection microscopy we assume that a spherical wave emanating from the point source scatters off the atoms of the object at a distance d from the source. An elongated carbon cluster is used to model a fiber, and a more extended gold cluster of several layers with a few hundred Au atoms each is used to describe the thin film. The image is formed at a screen, a distance D from the source, with $D \gg d$. We include single scattering only. With the origin of the coordi-

nate system at the point source, we write the spherical outgoing wave with wave number k as

$$\frac{\exp(ikr)}{r} = \frac{1}{N} \sum_{j=1}^N \frac{\exp(ik|\mathbf{r}-\mathbf{r}_j+\mathbf{r}_j|)}{|\mathbf{r}-\mathbf{r}_j+\mathbf{r}_j|}. \quad (1)$$

where \mathbf{r}_j is the position of the j th atom in the object; there are N atoms altogether. Next we expand (1) in spherical waves around each of the N atoms and, to include scattering from the atoms of the object, we replace the free wave function in this expansion by the scattering wave function. Using the asymptotic form of the scattering wave function for large separations, compared to the extent of the atomic scattering potential, we obtain

$$\psi_s(k, r) = -\frac{i}{2Nk} \sum_j \frac{\exp(ikr_j)}{r_j} \frac{\exp(ik\rho_j)}{\rho_j} \sum_l (2l+1)(S_l-1)P_l \left[\frac{(r \cos\theta_j - r_j)}{(r^2 + r_j^2 - 2rr_j \cos\theta_j)^{1/2}} \right], \quad (2)$$

where $\rho_j = |\mathbf{r}-\mathbf{r}_j|$ and the argument of the Legendre polynomial depends on the angle θ_j between r and r_j . Whereas the geometry of the object enters via the positions r_j of the constituent atoms, the scattering dynamics enters via the scattering matrix elements $S_l(k)$ in the l th partial waves. If $r_j \ll r$, (2) simplifies further; i.e., if we write $\psi_s = \exp(ikr)\bar{\psi}_s$, we get

$$\bar{\psi}_s(k, r) = -\frac{i}{2Nk} \sum_j \frac{\exp[ikr_j(\cos\theta_j - 1)]}{r_j|r-r_j|} \sum_l (2l+1)(S_l-1)P_l \left[\frac{(r \cos\theta_j - r_j)}{(r^2 + r_j^2 - 2rr_j \cos\theta_j)^{1/2}} \right]. \quad (3)$$

The contrast on the screen is given by the difference between the intensities with and without the object, i.e.,

$$I_s = I - r^{-2} = |\bar{\psi}_s|^2 + (2/r)\text{Re}(\bar{\psi}_s), \quad (4)$$

where $\text{Re}(\psi)$ denotes the real part of ψ . The first term is the direct scattering term. The second term arises from the interference between the scattered and the unscattered wave, and produces the holographic image. We note that the intensity from the interference terms is typically 2–4 orders of magnitude higher than the squared term.

Figure 2 shows typical experimental images. Panel (a) is the holographic image of a carbon fiber taken with the electron point source at a distance of about 1 μm . We observe typical interference fringes parallel to the fiber, but should also note the intensity modulation along the fiber. Local information is contained in this picture to the extent that we can roughly identify the position of the fiber. Panel (b) also shows the holographic pattern produced around the end of a fiber. Panels (c) and (d) are produced from thin gold films that are most likely less than 100 \AA thick, placed a few thousand angstroms from the electron point source. Atomic resolution is achieved with hexagonal and square unit cells clearly visible. The separation between the intensity spots is what one would expect with a magnification, D/d , of the order of 10^6 .

In Fig. 3 we reproduce a series of theoretical images that will help us interpret details of the experimental pictures. Panel (a) depicts one quadrant of the image calculated for a carbon fiber consisting of two layers of 151×5 carbon atom arranged in a fcc(100) structure with a lat-

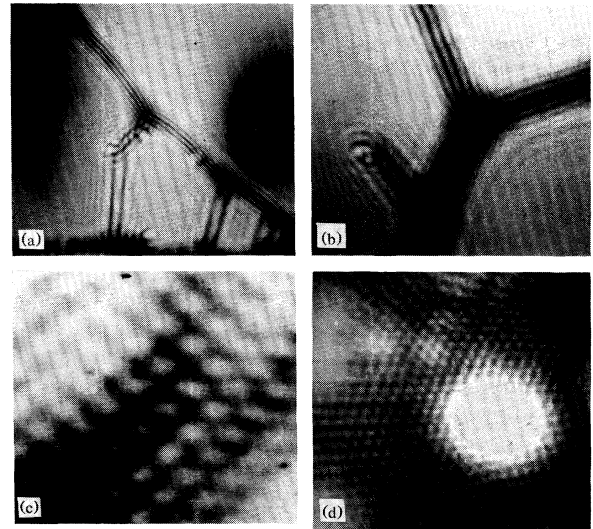


FIG. 2. (a),(b) Holograms of less than 100- \AA -wide carbon fibers, observed with electron energies of typically 20–100 eV. The smallest separation between interference fringes is 3–4 \AA . (c),(d) Transmission images of thin gold films taken with electron energies between 200 and 300 eV show the gold lattice atomically resolved. The bright part in (d) is due to a very thin part of the film that is overexposed owing to the limited dynamics of the detector system.

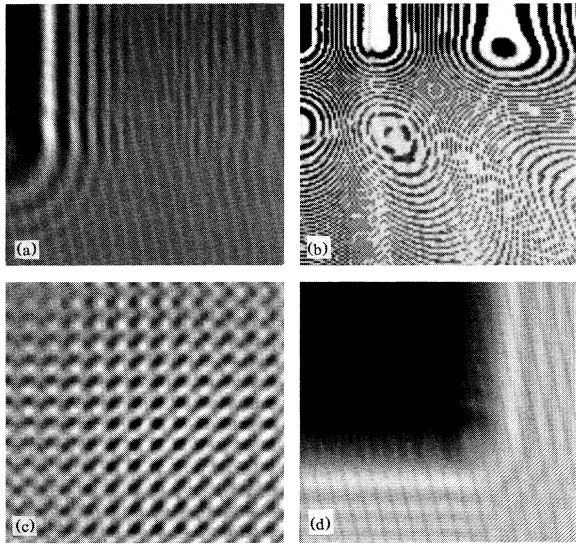


FIG. 3. Simulated holograms of (a),(b) carbon fibers and (c),(d) thin gold clusters. See text for detailed discussion.

tice constant $a = 2.5 \text{ \AA}$ and a lattice plane separation of 1.5 \AA . The electron energy was set at 50 eV and a magnification of 10^6 was achieved by choosing $d = 10^3 \text{ \AA}$ and $D = 10 \text{ cm}$. The four quadrants would represent the projection of an area of $320 \times 320 \text{ \AA}^2$ of the object plane. We note that the shadow around the fiber up to the first interference maximum is much larger than the true width of the fiber, namely, by roughly a factor of 10. Note the striations along the fiber, which are also noticeable in Fig. 2(b). Also note the beginning repetition (with lower intensity) of the image on the right-hand side of Fig. 3(a); this is more visible in a larger segment of the image, see panel (b), where we used a linear intensity scale to enhance the secondary fringes. Similar results have been obtained for a cluster of 151×31 carbon atoms and also for gold ribbons. The above calculations were performed by using realistic scattering phase shifts for carbon up to $l = 4$. In anticipation of attempts to invert the experimental holograms, we have tested the importance of the details of the phase shifts by repeating the calculations with s waves only. The main difference is a considerable brightening in the shadow area. On the other hand, the s -wave contribution may be adequate in the region far from the shadow area. Implications for the inversion procedure will be discussed in a future publication.

We now turn to the theoretical images [Figs. 3(c) and 3(d)] of Au clusters calculated at electron energies of 230 eV each with $d = 10^3 \text{ \AA}$ and $D = 10 \text{ cm}$. For panel (c) we chose a cluster of two layers with 101×101 atoms, showing a quarter of the area that corresponds to the projection of $70 \times 70 \text{ \AA}^2$. The atomic resolution with atoms spaced 2.88 \AA apart is clearly visible. Moreover, we can also see the effect of the second layer of the fcc(100)

structure, in particular in the lower left corner; however, the appearance of a hexagonal pattern should not be interpreted as evidence for fcc(111) exposure. Looking down the third row of intensity spots from the right, one might be tempted to see a merging of two atomic rows in an edge dislocation. It is important to remember that, although we achieved atomic resolution, these pictures are holographic in nature and can therefore not be interpreted with local ideas only. Panel (d) shows a more complete image, the quadrant being the image of an area of $226 \times 226 \text{ \AA}^2$ of the object film. Two features are noteworthy: (i) The interference fringes outside the cluster are folded into the image in the shadow of the cluster, producing intensity variations every few atomic rows; this feature is also present in experimental images. (ii) One can see intensity spots at more or less the proper separation outside the shadow area of the cluster, yet its actual size can be pinpointed to within one or two atomic distances.

To understand the feasibility of the direct observation of local structures, we have performed calculations for a Au cluster consisting of two halves, one exposing the fcc(111), the other the fcc(100) structure. One obviously does not expect a sharp division between the two structures in the images, but some zone of transition where both halves of the crystal contribute and pure symmetry pictures emerge far from the joining line. Again, there is evidence for this in experimental images. As a last example, we mention a calculation in which we removed some atoms from the cluster to model a hole. Again, one can identify this local information in the image, suggesting that with some experience one will be able to develop enough intuition to interpret images without having to resort to theory in every instance.

We have demonstrated, both experimentally and theoretically, that the low-energy-electron projection microscope yields holographic images that can be pushed to yield atomic resolution for a crystalline film. It now remains to develop the criteria for the latter: Atomic resolution can be achieved if enough atoms in the film contribute to constructive interference in the center of the image. This requires that the path difference Δs in the spherical wave at the edge and at the center of the object film is much larger than the wavelength of the electrons, λ . We get

$$\Delta s = (d^2 + \frac{1}{4} w^2)^{1/2} - d \approx w^2/8d \gg \lambda, \quad (5)$$

where w is the width of the object film.

To obtain an undistorted picture of atomic resolution a further requirement is that the first diffracted beam from the edges of the object film is outside the zero beam from the center of the film. This is achieved if $w/2d \ll \lambda/a$, where a is the lattice constant. Thus we can say that a crystalline film can be imaged with atomic resolution for geometries where

$$\sqrt{d\lambda} \ll \frac{1}{2} w \ll \lambda d/a. \quad (6)$$

Within these limits, the image will contain direct visual evidence of atomic structure without the need for comparison to model calculations or reconstruction of the wave front at the object.

To conclude, we would like to discuss some of the immediate tasks at hand. The best resolution is of little use if it is not also related to a high contrast in the imaging process. For the low-energy-electron projection microscope even light atoms such as carbon give rise to high phase contrast. We have evidence that the new microscope is ideally suited for imaging large molecules of biological interest. There is also far less radiation damage than in conventional high-energy transmission electron microscopy. On the theoretical side, the assumption of single scattering must be investigated, although we do not anticipate dramatic changes. More importantly, the inversion of the holographic images must be attempted. Our very simple final formula is very suggestive in this regard. However, we would like to point out that such an inversion procedure, although desirable, is not absolutely necessary, as the theory developed so far allows the straightforward calculation of images for comparison with experimental ones.

Werner Stocker made major contributions to the technical development of the projection microscope. Those of us involved in the experimental work gratefully acknowledge Heini Rohrer's continuous support of the project. We like to thank Michael Nicksch for helping us become familiar with the IBM Zurich Distributed Computing environment. The work has been supported by a Joint Research Agreement between the Dalhousie University and the IBM Zurich Research Laboratory. We also acknowledge a grant funded by the Network of Centres of Excellence Programme in association with the Natural Sciences and Engineering Research Council of Canada.

-
- [1] D. Gabor, *Nature (London)* **161**, 777 (1948).
 - [2] H. Lichte, *Ultramicroscopy* **20**, 293 (1986); A. Tonomura, *Phys. Today* **43**, No. 4, 22 (1990).
 - [3] H.-W. Fink, *Phys. Scr.* **38**, 260 (1988).
 - [4] W. Stocker, H.-W. Fink, and R. Morin, *Ultramicroscopy* **31**, 379 (1989); H.-W. Fink, W. Stocker, and H. Schmid, *Phys. Rev. Lett.* **65**, 1204 (1990).

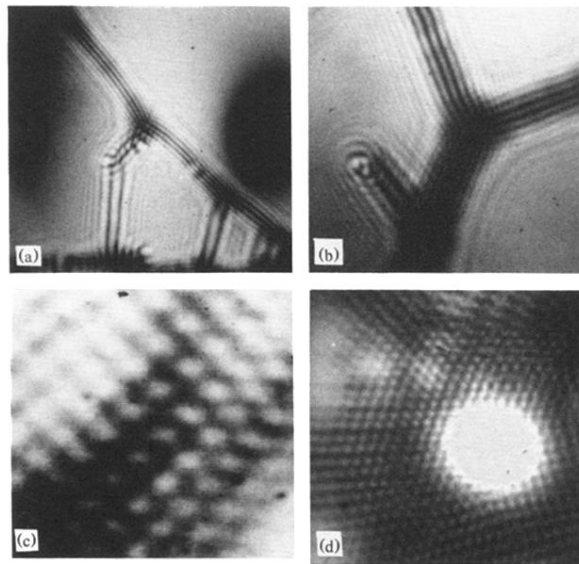


FIG. 2. (a),(b) Holograms of less than 100-Å-wide carbon fibers, observed with electron energies of typically 20–100 eV. The smallest separation between interference fringes is 3–4 Å. (c),(d) Transmission images of thin gold films taken with electron energies between 200 and 300 eV show the gold lattice atomically resolved. The bright part in (d) is due to a very thin part of the film that is overexposed owing to the limited dynamics of the detector system.

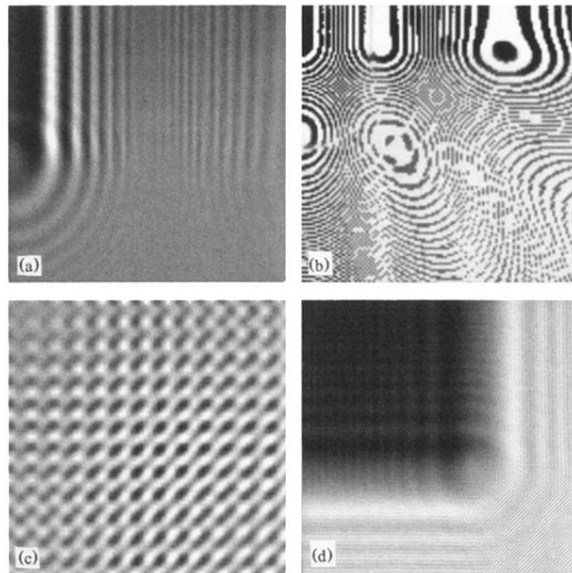


FIG. 3. Simulated holograms of (a),(b) carbon fibers and (c),(d) thin gold clusters. See text for detailed discussion.